POLITECNICO DI TORINO
Repository ISTITUZIONALE

Lumped-Parameter Models Comparison for Natural Ventilation Analyses in Buildings at Urban Scale

Original
Lumped-Parameter Models Comparison for Natural Ventilation Analyses in Buildings at Urban Scale / Usta, Y., Ng, L., Santantonio, S., Mutani, G.. - In: ENERGIES. - ISSN 1996-1073. - ELETTRONICO. - 18:9(2025), pp. 1-26. [10.3390/en18092352]

Availability:
This version is available at: 11583/3000293 since: 2025-05-19T20:53:03Z

Publisher:
Multidisciplinary Digital Publishing Institute (MDPI)

Published
DOI:10.3390/en18092352

Terms of use:

This article is made available under terms and conditions as specified in the corresponding bibliographic description in the repository

Publisher copyright

(Article begins on next page)

25 November 2026

energies

MDPI

Article

Lumped-Parameter Models Comparison for Natural Ventilation Analyses in Buildings at Urban Scale

Yasemin Usta [1], Lisa Ng [2], Silvia Santantonio [1] and Guglielmina Mutani [1,*]

[1] Department of Energy, Politecnico di Torino, 10129 Torino, Italy; yasemin.usta@polito.it (Y.U.); silvia.santantonio@outlook.it (S.S.)
[2] National Institute of Standards and Technology, Gaithersburg, MD 20899, USA; lisa.ng@nist.gov
* Correspondence: guglielmina.mutani@polito.it

Abstract: This study validates a three-zone lumped-parameter airflow model for Urban Building Energy Modeling, focusing on its accuracy in estimating air change rates caused by natural ventilation, referred to here as air change rate. The model incorporates urban-scale variables like canyon geometry and roughness elements for the accurate prediction of building infiltration, which is an important variable in building energy consumption. Air change rate predictions from the three-zone lumped-parameter model are compared against results from a three-zone CONTAM model across a range of weather scenarios. The study also examines the impact of building level of detail on air change rates. Results demonstrate that the three-zone lumped-parameter model achieves reasonable accuracy, with a maximum Mean Absolute Error of 0.1 h^{-1} in winter and 0.03 h^{-1} in summer compared to three-zone CONTAM model, while maintaining computational efficiency for urban-scale energy consumption simulations. However, its applicability is limited to buildings within urban canyons rather than detached structures, due to the assumptions made in the methodology of the three-zone lumped-parameter model. The results also showed that the model had lower errors for low to mid-rise buildings since the simplification of a detailed high-rise building into a three-zone model alters the buoyancy effect; a 4-story building showed Mean Absolute Percentage Error of 7% and 5% for a typical winter and summer day respectively when a detailed and simplified three-zone models are compared, while the error for a 16-story building were 18% and 12%. The results of building air change rates are used as input data in an hourly energy consumption model at urban scale and validated against measured hourly consumption to test the effect of the calculated urban-scale hourly air change rates.

Keywords: building ventilation; infiltrations; lumped-parameter model; ACR; CONTAM; Urban Building Energy Modeling; place-based approach

check for updates

Academic Editor: Boris Igor Palella

Received: 9 March 2025
Revised: 16 April 2025
Accepted: 30 April 2025
Published: 4 May 2025

Citation: Usta, Y.; Ng, L.; Santantonio, S.; Mutani, G. Lumped-Parameter Models Comparison for Natural Ventilation Analyses in Buildings at Urban Scale. *Energies* **2025**, *18*, 2352. https://doi.org/10.3390/en18092352

Copyright: © 2025 by the authors. Licensee MDPI, Basel, Switzerland. This article is an open access article distributed under the terms and conditions of the Creative Commons Attribution (CC BY) license (https://creativecommons.org/licenses/by/4.0/).

1. Introduction

Building energy consumption represents the largest share of urban energy use. According to the International Energy Agency (IEA), operational energy use in buildings accounts for about 30% of global final energy consumption [1]. In the United States, buildings are responsible for 40% of total energy use, including 75% of all electricity use [2].

Building energy modeling (BEM) has emerged as a powerful decision-support tool, enabling the assessment of energy efficiency strategies and identifying conditions that cause higher energy consumption. For instance, the U.S. Department of Energy highlights BEM's adaptability, remarking on its applications, both for new buildings and retrofit design, to develop building energy-efficiency codes and decision policies [3]. However, BEM usually

focuses on individual buildings and detailed energy systems, but the complexity of the urban environment—particularly the influence of surrounding elements such as buildings and trees—demands more comprehensive modeling approaches.

Urban Building Energy Modeling (UBEM) addresses this gap by extending energy analysis to an urban scale, accounting for physical surroundings, microclimatic conditions, and building-specific characteristics. Recent reviews have highlighted both the significance and potential of UBEMs, while also addressing the challenges they face and suggesting ways to enhance their robustness [4,5]. UBEM incorporates factors such as shading effects, wind dynamics, and urban density to provide a comprehensive understanding of energy consumption and production. For example, shadows from different urban elements can impact the effectiveness of solar technologies [6], while modifications in wind speed caused by surrounding structures or roughness elements can influence ventilation and airflow rates [7–9]. Recent studies have also emphasized the critical role of occupant behavior in urban-scale modeling, highlighting the need for detailed, data-driven occupancy models to reduce simulation uncertainties and enhance the accuracy of energy demand predictions [10]. These interdependencies highlight the importance and potential of UBEM in identifying scenarios that improve an efficient use of energy at urban scale.

Given the complexity of urban environments and the volume of data required for large-scale analysis, a flexible, time-efficient, and scalable modeling framework is essential for analyzing large urban environments. In this context, process-driven UBEM provides an effective approach to calculate building energy use based on physical descriptions and local weather data. These models can rely on available open-source data for building details such as thermal transmittance and geometric data and often implement the assumption of fixed air change rate (ACR) that are based on a building permeability which is associated with construction period.

However, the assumption of a constant ACR does not reflect real-world conditions, as air infiltration is influenced by factors not only related to building envelope airtightness but also by issues such as the wind pressure on the building envelope and indoor-outdoor temperature gradients. A study that compared experimental methods for estimating infiltration rates highlighted the variability introduced by wind speed, wind direction, and temperature gradients [11]. The results emphasized that while experimental methods, such as CO_2, decay provide valuable insights on infiltration, they cannot fully account for the complexities of urban environments, including the influence of urban geometry on wind patterns.

The presented work contributes to broader research that aims to enhance the performance of an hourly process-driven and place-based UBEM. Initial efforts were made to improve ACR calculations focused on scenarios that involve using fixed ACR values, day/night adjustments, and adding window operation schedule, which all demonstrated significant impacts on energy consumption [6]. The second step refines ACR calculations by correcting wind speed inside the urban canyon to incorporate the effects of urban geometry on airflow dynamics. Lastly, the model is further developed to calculate energy consumption by representing each building as three interconnected zones, which is intended to better predict performance in large scales applications in conjunction with urban effects [12]. Validating this modeling approach will mark a critical step toward improving urban-scale energy consumption analysis.

Finally, in this work, the term **air change rate (ACR)** is used to describe the rate of air flow due to natural infiltration. While Air Change per Hour (ACH) is frequently applied in both mechanical and natural ventilation contexts, ACR specifically refers to air changes resulting from natural forces such as wind and temperature differences, providing a more accurate description of the phenomenon under consideration.

2. Objective of the Work

The primary aim of this analysis is to assess the accuracy of an already existing simplified three-zone lumped-parameter model [12] by comparing its results with CONTAM, a multizone airflow and contaminant transport simulation program [13]. The methodology presented in [12] calculated the ACR for a simplified building geometry by considering the surrounding built environment, which affects wind speed inside urban canyons due to urban roughness elements, as well as indoor conditions inside buildings.

The novelty of this work lies in analyzing the impact of building level of detail (LoD) on building ACR calculations and evaluating whether the three-zone lumped-parameter model, with its simplified representation of building geometry, is effective in estimating ACR for energy use prediction. This assessment will help define the applicability and limitations of the three-zone lumped-parameter model's methodology in urban scale natural ventilation load assessment.

The broader goal of this analysis is to support strategies to effectively use energy in urban areas. This will be enabled by developing an effective model for calculating hourly ACR as a function of urban geometry and local weather conditions, which can be then used as an input for energy consumption modeling at urban scale, while also optimizing simulation costs. By incorporating the effects of urban street canyons on wind speed and airflow dynamics, this methodology seeks to provide a more accurate building ACR input for UBEM, replacing widely used fixed assumptions.

3. Methods

The workflow followed in this analysis is outlined in Figure 1. The buildings used in the analysis are provided in Section 3.1. The study begins with providing a Level of Detail (LoD) analysis (Section 3.2) using CONTAM. This analysis aims to highlight the effect of simplifying a detailed building into three zones on the results of building ACR.

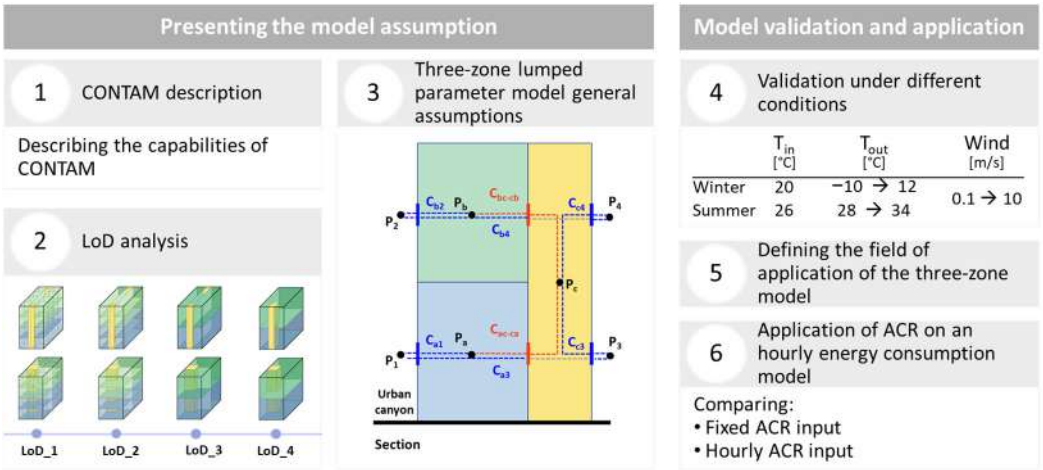

Figure 1. Manuscript workflow.

Section 3.3 provides an overview of the general assumptions made in the existing three-zone lumped-parameter model [12], and the boundary conditions used for the validation: 10 different indoor-outdoor temperature scenarios are tested under 12 wind speeds. The results of the defined boundary conditions from the three-zone lumped parameter model are compared with a three-zone CONTAM model. The results of both the LoD analysis and the validation are discussed in Section 4.

Following the validation, the study explores the potential applications of the proposed modeling approach, including its limitations, in Section 4.3.

Finally, Section 4.4 demonstrates the application of using an hourly ACR from a three-zone lumped-parameter model in estimating hourly energy consumption for space heating in residential buildings by comparing it against using fixed ACR values. The hourly energy consumption results of using hourly and fixed ACR are compared with real measured consumption data.

3.1. Analyzed Buildings

3.1.1. Midrise Prototype Building

The midrise prototype building is selected from the detailed CONTAM models developed by the National Institute of Standards and Technologies (NIST) and derived from U.S. Department of Energy (DOE) reference building models [14].

Figure 2 shows the typical floor plan of the prototype building. In this building the corridor divides the apartments/office across two opposite facades, thus, there is no cross ventilation for a single unit. The staircase and elevator are located at each end of the corridor resulting in two shafts. The building has 4 floors, each with a height of 3.05 m.

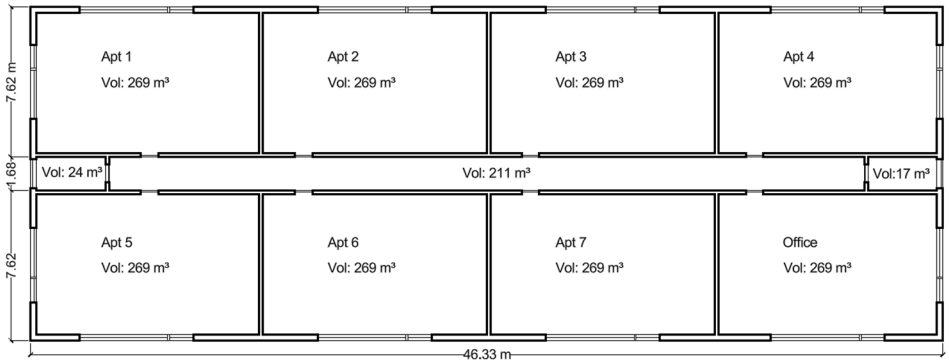

Figure 2. Typical floor plan for the midrise prototype building.

3.1.2. Turin Building

The building is a typical condominium built before 1918, located on a large street canyon (approximately 45 m wide), with adjacent buildings on both sides. It has two opposing facades: a canyon façade and a courtyard façade on the same side of the buildings as the staircase, which provides each apartment with cross ventilation. Unlike the prototype building, the staircase and the elevator are in a single shaft.

The building consists of 5 floors: a ground floor with vehicle access to the courtyard and 4 floors with layout as shown in Figure 3. The ground floor is excluded from the ACR calculations, as it is generally not used for residential purposes. The floor height for the typical floors is 3.3 m.

3.2. Level of Detail (LoD) Analysis

3.2.1. CONTAM

CONTAM (version 3.4.0.1) is a multizone modeling software, developed at the National Institute of Standards and Technology (NIST) [15]. CONTAM accounts for room-to-room, infiltration, and exfiltration airflows driven by temperature-induced pressures (i.e., stack effect), wind pressures acting on the building exterior, and mechanically-driven pressure differences (i.e., heating, ventilation, and air-conditioning system flows). The meteorological variables considered in the calculation of airflow rates are the ambient temperature [K], barometric pressure [Pa], wind speed [m/s], and wind direction [°].

CONTAM is able to perform whole-building simulations for periods of up to one year with an assumption that pressures only vary hydrostatically. Thus, its computational requirements are not as intensive as using other airflow simulation methods like

Computational Fluid Dynamics (CFD). CONTAM has been validated in terms of program integrity [16], laboratory experiments [17], and field studies in residential buildings [18,19]. It was also used to compare real-time infiltration estimates between detailed and simplified (e.g., single zone) models of two residential test houses at NIST [20]. Depending on the tightness of the test house and the simulated weather, the simplified models could capture the whole-building infiltration rate as well as the detailed model for the buildings studied.

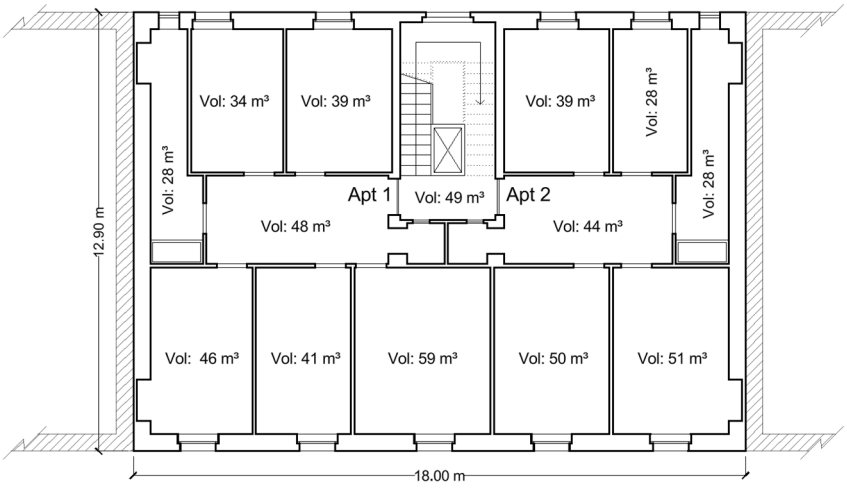

Figure 3. Typical floor plan for Turin building.

3.2.2. LoD Steps

The LoD analysis is performed using CONTAM and aims to evaluate the impact of building simplification into three zones by comparing the ACR results between a detailed building geometry and a simplified three-zone building: two heated zones representing the upper and lower levels of the building and an unheated shaft connecting them.

The building geometry is simplified according to the schematization provided in Figure 4, which outlines the LoD steps used for both buildings. The aim of including two buildings in the LoD analysis is to test the effects of building simplification on models with different floor plans and climate zones.

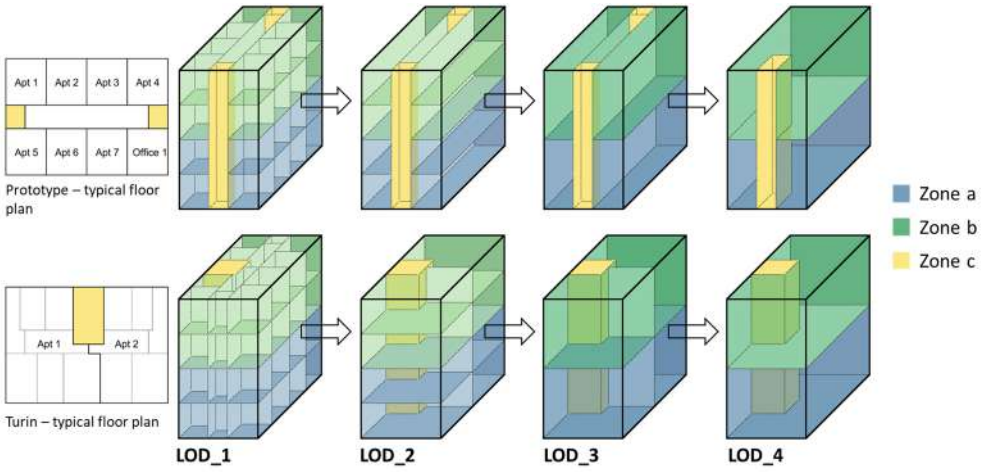

Figure 4. Level of Detail steps to achieve three-zone model.

The simplification starts with a detailed building geometry, considering all airflow elements that represent a real case (including leakages from windows, floors, internal/external walls, and roof). Then the building geometry is progressively reduced, arriving at the three-

zone model. In the detailed building step (LoD_1), the internal doors within each apartment are assumed to be open, while the apartment/shaft doors are considered closed.

For the prototype building, the simplification starts with removing the partitions between the apartments in LoD_2, followed by merging the building floors into two levels in LoD_3, and finally removing the corridor and merging the shafts into single shaft to arrive at three-zones in LoD_4.

For the building in Turin, the process starts by removing the internal partitions within each apartment in LoD_2, followed by merging the building floors into two levels in LoD_3, and finally removing the partition between the apartments in LoD_4.

Although the simplification steps differ between the two buildings, the main approach remains consistent: both buildings are simplified into a three-zone model, with two zones representing the upper and lower levels of the building and one shaft connecting them [21]. The results of this building simplification on ACR values are provided in Section 4.1.

3.2.3. LoD Models in CONTAM

For each analyzed building, the four LoD steps are modeled in CONTAM. Figures 5 and 6 provide CONTAM models for LoD_1 and LoD_4 only, to allow the direct comparison between the detailed and simplified models. The figures provide the models for both buildings with areas and volumes of each zone before and after the simplification (Figure a and b respectively). The airflow elements considered in this analysis are mainly the leakage from the envelope (in blue), the closed-door leakage (in red) and the floor leakage (in green). However, it should be highlighted that in the three-zone lumped-parameter model there is no leakage from the horizontal elements (floors, roof). To account for this behavior, it is represented as LoD_4″, which is the same as LoD_4 but excludes the leakage from the roof and between floors of the apartments.

In the prototype building, as shown in Figure 5a, there are no partitions within each apartment. Consequently, the only internal doors are the apartment/shaft doors (in red).

For the building in Turin, Figure 6a, there are two internal door types: within each apartment (in pink), which are considered open, and the apartment/shaft doors (in red), which are considered closed.

The leakage from the building envelope is obtained from available references related to whole building airtightness testing results [22], which are usually provided as normalized airflow rates, e.g., L/s/m^2 @75Pa.

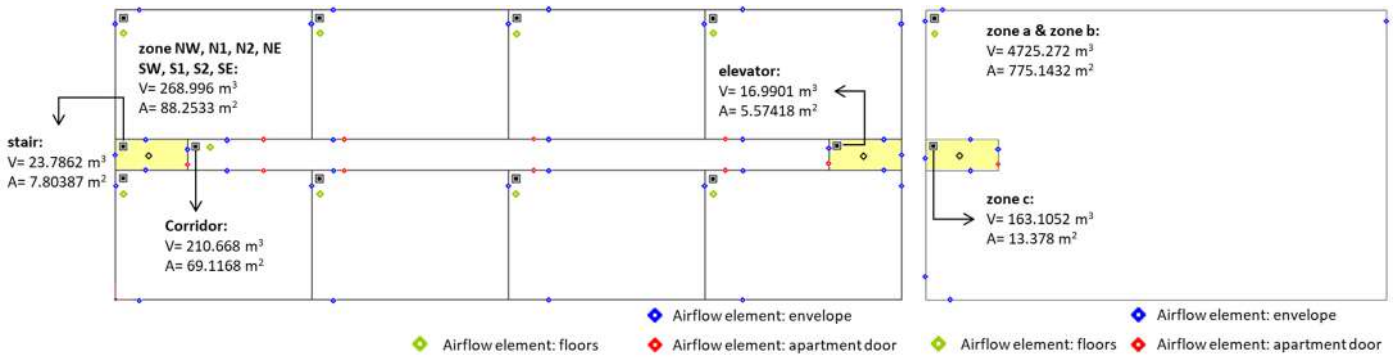

LoD_1 (**a**) LoD_4 (**b**)

Figure 5. Prototype building CONTAM model for LoD_1 (**a**) and LoD_4 (**b**).

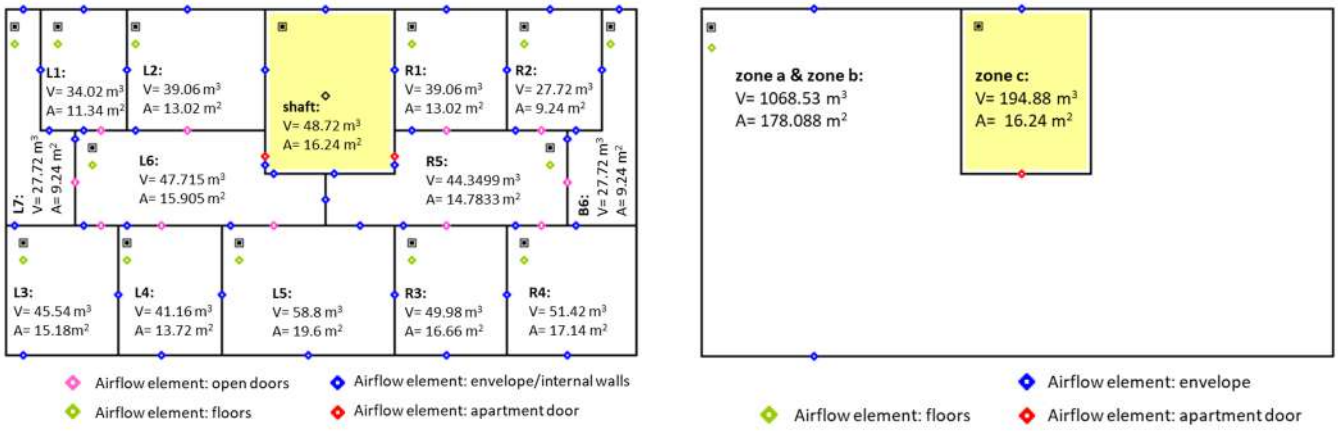

LoD_1 (**a**) LoD_4 (**b**)

Figure 6. Turin building CONTAM model for LoD_1 (**a**) and LoD_4 (**b**).

Having this normalized value, it was possible to calculate the leakage area A_L (cm^2/m^2) as an input for the flow elements in CONTAM using Equation (1) [14]. This leakage area is typically provided under reference test conditions, which include the discharge coefficient (C_d), flow exponent (n), and pressure difference (ΔP).

$$Q = \frac{C_d A_L}{10000} \cdot \sqrt{\frac{2}{\rho}} \cdot (\Delta P_r)^{0.5-n} \cdot \Delta P^n \quad (1)$$

where:

Q_r is the predicted airflow rate at ΔP_r (from pressurization test data) [$L/s/m^2$]
C_d is the discharge coefficient [-], used here as 1
A_L is the leakage area [cm^2/m^2]
ρ is the air density [kg/m^3]
ΔP_r is the reference pressure difference (from pressurization test data) [Pa]
n is the flow exponent [-], used here as 0.65
ΔP is the pressure difference, used here as 4 Pa.

The value of the flow exponent depends on the type of opening, whether it is large or small [15]. Generally, the values are near 0.65 for small cracks, which can be used to represent the leakage from window, door, and wall cracks [15,22]. For the discharge coefficient (C_d), one of the common reference conditions for small leakage areas is 1.0 at ΔP = 4 Pa [15,22]. Although these values can be used for small openings, Equation (1) can be used to convert reference building airflow rates for the required boundary conditions.

For the prototype building, the airtightness value used is 3.83 $L/s/m^2$ @75 Pa. For the building in Turin, the whole building airtightness value is 3.09 $L/s/m^2$ @75 Pa, which is the average value for multi-unit residential buildings (MURBs), determined from airtightness tests performed on 113 buildings [22].

Table 1 provides the leakage elements used in CONTAM for each building. The closed apartment/shaft doors in the prototype building are modeled in CONTAM using the Powerlaw Model: Orifice airflow element type.

Table 1. Leakage data of the analyzed buildings.

Envelope (walls, floors, roof): Powerlaw Model: Leakage area			
	Prototype	Turin	
Leakage per unit area [cm^2/m^2]	2.208	1.783	
Discharge coefficient [-]	1	1	
Flow exponent [-]	0.65	0.65	
Pressure difference [Pa]	4	4	
Internal doors			
Prototype		Turin	
Apartment/shaft doors: Powerlaw Model: Orifice		Internal doors (within apartments): Two-way Model: Single-opening	
Cross-sectional area [m^2]	0.023	Height [m]	2.2
Flow exponent [-]	0.5	Width [m]	0.9
Discharge coefficient [-]	0.6	Discharge coefficient [-]	0.78
Hydraulic diameter [m]	0.172	Apartment/shaft doors: Powerlaw Model: $F = C(\Delta P)^n$	
Reynold number [-]	30	Flow coefficient (C) [-]	Equation (2)
		Flow exponent (n) [-]	0.65

For the building in Turin, having two internal door elements, the open doors within each apartment are modeled using two-way model: Single-opening, and for the closed apartment/shaft doors using a Powerlaw Model: $F = C(\Delta P)^n$. For the latter, the flow exponent (n) is 0.65 and the flow coefficient (C) is calculated using Equation (2) assuming a typical leakage area of 12 cm^2/m^2 for each door. This estimate represents a loosely sealed element, considering construction period of the building [23,24].

The flow coefficient $C_{opening}$ [$kg \cdot s^{-1} \cdot Pa^{-n}$] for the shaft door in the Turin building is calculated using Equation (2). It is related to the leakage area ($A_{leakage}$) calculated using the typical leakage area values (A_L) available in standards or local databases [22–24].

$$C_{opening} = C_{d,opening} \cdot A_{leakage} \cdot (2 \cdot \rho)^{\frac{1}{2}} A_{leakage} = A_L \cdot A_{opening} \quad (2)$$

where:

$C_{d,opening}$ is the discharge coefficient of the opening [-], used here as 0.65
$A_{leakage}$ is the leakage area of the opening [m^2]
ρ is the air density [kg/m^3]
A_L is the leakage area [cm^2/m^2], used here as 12 cm^2/m^2
$A_{opening}$ is the opening area of the airflow element [m^2], used here as 1.98 m^2.

3.2.4. LoD Indoor Temperature and Weather Data

For the LoD analysis, a simulation for a representative winter and summer day with a one-hour timestep is used to calculate the hourly ACR. Although the overall simulation is annual, each hourly interval is solved under steady-state conditions.

The setpoint temperatures for the heated zones are 20 °C in winter and 26 °C in summer, while for the shaft the temperature is calculated using the equation provided in Table 2. These temperature schedules are assigned to each zone using continuous value files (.cvf) in CONTAM.

Table 2. Internal conditions of the analyzed buildings.

Season	Temperature [°C]	
	Heated Zones (a&b)	Shaft (Zone c)
Winter	20	$T_{sh} = T_{out} + b_{tr,u}^{*} \cdot (T_{in} - T_{out})$
Summer	26	

* $b_{tr,u}$: correction factor for confined spaces (shaft with one wall facing outwards), equals to 0.4 (Table 5 in the Appendix A of the Italian standard UNI/TS 11300-1: 2014 [25]).

The weather data used for both buildings are sourced from the EnergyPlus weather database [26], and subsequently converted from ".epw" format to CONTAM-compatible ".wth" format using the CONTAM weather file creator [27].

Figure 7 provides the outdoor air temperature (in red) and wind speed (in black) for a representative winter and summer day. These graphs show that the results of the three-zone model simplification will be analyzed considering different weather conditions: tropical (with hot and humid summers) in Miami for the prototype building and continental temperate in Turin. Both analyzed buildings, midrise and Turin, are simulated using the two weather files to compare the effects of climate and building geometry on the ACR results.

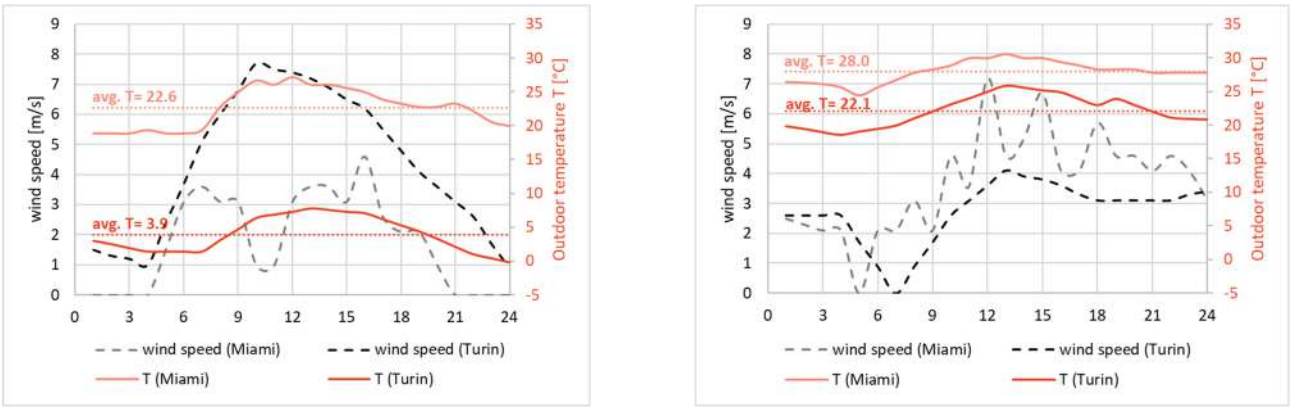

(**a**) Winter (**b**) Summer

Figure 7. Hourly weather data for Turin and Miami used in LoD analysis.

The wind pressure coefficients used in this vary as a function of the angle of the envelope flow paths relative to wind direction only [28], i.e., coefficients do not vary with height.

3.3. Three-Zone Lumped-Parameter Model

3.3.1. General Aim

The main aim of the three-zone lumped-parameter model being validated was to simplify a building into three zones to enable urban scale natural ventilation load assessments in energy consumption calculations, while minimizing simulation costs [12]. The existing model was used in this work with few impoorvements, e.g., neglecting the dynamic component of the pressure in the internal zones. The results of this simplification of the building geometry on the ACR results are discussed in Section 4.2.

The three-zone lumped-parameter model is used to consider outdoor airflow dynamics within urban street canyons, which are significantly influenced by the urban geometry (i.e., height-to-width ratio H/W).

3.3.2. Corrected Wind Speed

In this model, a Geographic Information System (GIS)-based approach is used to calculate aerodynamic roughness parameters that influence wind dynamics within urban areas. QGIS (Quantum Geographic Information System) is an open-source tool used to analyze and visualize spatial data. It supports a wide range of geospatial formats and provides various tools for geoprocessing and spatial analysis. To calculate the aerodynamic and morphometric parameters, the Urban Multi-scale Environmental Predictor (UMEP) plug-in within QGIS was employed [29]. This tool calculates aerodynamic and morphometric parameters using a 3D representation of the urban environment, i.e., digital surface models (DSM) and digital elevation models (DEM). To calculate the aerodynamic parameters, including the displacement height (z_d) and roughness length (z_0), the Morphometric Calculator tool within the plugin applies six different roughness calculation methods based on morphometric parameters [30]. Depending on the selected method, the calculation incorporates one or more morphometric parameters: plan area density (λp), frontal area ratio (λf), average building height (zH), maximum building height (zHmax), and height variability (zHstd). Among the six methods, the Kanda method is suggested for dense urban environments, as it incorporates all five morphometric parameters for the calculation of z_d and z_0 [31].

The primary parameter obtained from UMEP is the displacement height (z_d), which is determined as a function of the built environment and wind direction. Knowing the displacement height (z_d) in front of each building, the wind speed can be adjusted using the logarithmic law for buildings above z_d, where the flow is less turbulent and CFD simulations for buildings below z_d, in which turbulent flows occur. Most buildings in dense urban environments have turbulent airflow inside the canyon, thus requiring CFD simulations for the wind speed adjustment [32].

Considering the high simulation costs of CFD, this wind speed correction methods used to reduce the number of simulations by categorizing wind effects related to urban canyons according to height-to-width ratio (H/W). Generally, the canyons in a city can be defined as large, medium, and narrow. These canyon categories and weather scenarios for the CFD simulations are presented in Figure 8. The simulations are performed for four effects considering the presence or absence of wind and temperature gradient between opposing building facades in the urban canyon, four representative seasons, and four positions of the building surfaces with respect to wind direction and solar irradiation; windward/leeward with warm/cold façade. Thus, as illustrated in Figure 8, 192 CFD simulations are performed, i.e., 64 simulations for each canyon geometry category. The results of the CFD simulations are used as boundary conditions to calculate the ACR for each building in the city considering its canyon category, building position, and the weather conditions during each hour simulated.

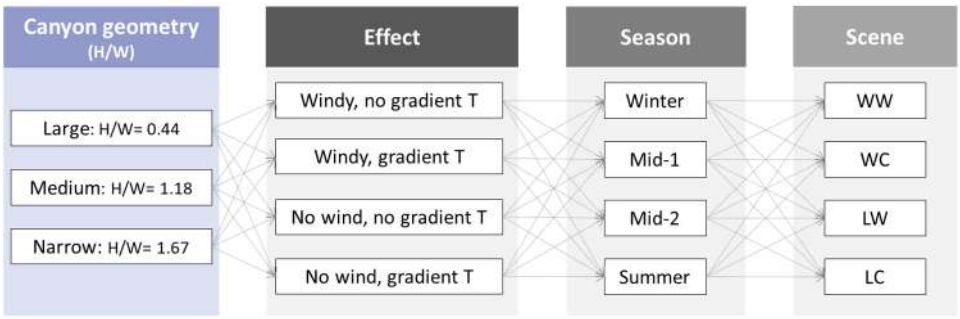

Figure 8. CFD simulation scenarios: WW: windward warm façade, WC: windward cold façade, LW: leeward warm façade, LC: leeward cold façade.

3.3.3. Three-Zone Building Simplification

Geometrical Simplification

The corrected wind speed explained previously is used as input data for a three-zone representation of each building in a city. The three interconnected zones shown in Figure 9 include two heated zones that correspond to the lower and upper apartment levels (zone a and b) and an unheated shaft connecting them (zone). The airflow connections between zones are depicted as thick lines (red for internal and blue for envelope connections) that are labeled with their flow coefficient (e.g., C_{a1}). The nodes represented as black dots in Figure 9 are characterized by steady-state conditions and air pressures, following the available multizone airflow modeling tools, e.g., CONTAM and COMIS [33], as well as to simplify the modeling approach which will be applied on urban scale.

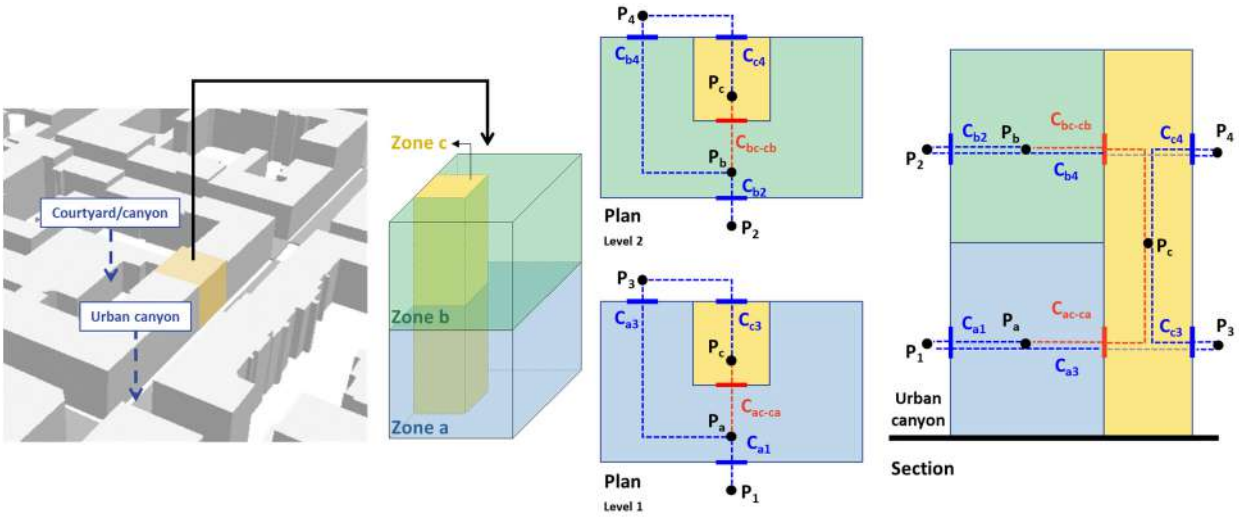

Figure 9. Three-zone lumped-parameter model schematization.

It was assumed that there was no airflow between zones a and b, the roof of zone b and c, and between the common walls of each building with its adjacent buildings. Thus, the stack effect is accounted for only in zone c. This assumption reduces the number of airflow path links, thereby minimizing simulation time for urban-scale analysis.

Physical Assumptions

In order to solve for the unknown internal zone pressures (P_a, P_b, P_c), a set of steady-state mass airflow conservation equations were applied as shown in Equations (3) and (4). The flow coefficient (C) is calculated for each link using Equation (2) provided previously. This three-zone, nonlinear system of equations was solved using MATLAB (version R2023b) applying the *fsolve* function and setting initial values and tolerance criteria [12,34].

$$\begin{cases} \dot{m}_{a1} + \dot{m}_{a3} + \dot{m}_{ac} = 0 \\ \dot{m}_{b2} + \dot{m}_{b4} + \dot{m}_{bc} = 0 \\ \dot{m}_{ca} + \dot{m}_{cb} + \dot{m}_{c3} + \dot{m}_{c4} = 0 \end{cases} \quad (3)$$

$$\begin{cases} C_{a1}\,(\Delta P_{a1})^n + C_{a3}\,(\Delta P_{a3})^n + C_{ac}\,(\Delta P_{ac})^n = 0 \\ C_{b2}\,(\Delta P_{b2})^n + C_{b4}\,(\Delta P_{b4})^n + C_{bc}\,(\Delta P_{bc})^n = 0 \\ C_{ca}\,(\Delta P_{ca})^n + C_{cb}\,(\Delta P_{cb})^n + C_{c3}\,(\Delta P_{c3})^n + C_{c4}\,(\Delta P_{c4})^n = 0 \end{cases} \quad (4)$$

where:

C is the flow coefficient [$kg \cdot s^{-1} \cdot Pa^{-n}$]
$\dot{m}$ is the airflow rate [kg/s]
ΔP is the total pressure difference [Pa].

The presented two-step approach—CFD simulations to calculate outside wind speed within the urban canyon, followed by a three-zone airflow model to estimate ACR—links urban-scale wind dynamics and building-level airflow rates, enabling the assessment of building infiltration in dense urban environments.

Validation with CONTAM

The validation aims to test the three-zone lumped-parameter model, explained in the previous section, with a three-zone CONTAM model to test the accuracy of the implemented model. For this validation, the building in Turin is used.

The validation is performed with a steady-state simulation using a range of weather data, which is derived from the hourly weather data presented previously in Section 3.2.4. This range is defined to ensure that the model is tested under different conditions, including extreme temperature cases (T_{out}), i.e., −10 °C to 34 °C and extreme wind velocity cases (W_s), i.e., 10 m/s as provided in Table 3.

Table 3. Weather data used for the model validation.

			Winter					**Summer**		
T_{out} [°C]	−10	−5	0	3	7	12	24	28	30	34
W_s [m/s]	0.1, 0.5, 1 → 10 (with an increment of 1 for each simulation)									

The indoor setpoint temperatures remain the same as 20 °C and 26 °C for winter and summer, respectively, for the heated zones, while for the shaft it is calculated using the equation provided previously in Table 2.

4. Results

This section presents the performance of the three-zone lumped-parameter model, implemented for urban scale energy analysis, through two steps. First, analyzing the impact of LoD on building ACR results, then validating the three-zone lumped-parameter model with a three-zone CONTAM model under a range of weather conditions. This is followed by highlighting the field of application of the presented methodology. Finally, an example application of this methodology on a residential building for space heating is provided in Section 4.4.

To assess the model's performance, the Mean Absolute Error (MAE) and the Mean Absolute Percentage Error (MAPE) are calculated using Equation (5). These metrics are applied to compare the difference in ACR results between a detailed CONTAM building model (LoD_1) and three-zone CONTAM models (LoD_4 and LoD_4″) and to assess the difference in building ACR between the three-zone lumped-parameter model and a three-zone CONTAM model.

$$MAE = \frac{1}{n}\sum_{i=1}^{n}|y - \hat{y}| MAPE = \frac{1}{n}\sum_{i=1}^{n}\left|\frac{y - \hat{y}}{y}\right| \times 100 \quad (5)$$

where:

y is the actual value
$\hat{y}$ is the predicted value
n is the total number of observations.

4.1. Level of Detail (LoD) Analysis Using CONTAM

4.1.1. Midrise Prototype Building Results

The results of the ACR analysis for different LoD are presented in Figures 10 and 11, for typical winter and summer days, in Miami. LoD_1 and LoD_2 exhibit similar results, indicating that internal partitions have a negligible effect on the ACR. The most significant change occurs in LoD_3, where the building floors are merged into two representative zones (upper and lower levels). This simplification increases the ACR overall due to the absence of internal obstructions. Additionally, it likely alters the buoyancy effect, as leakage in the detailed representation is assumed to occur at the midpoint of each floor height, whereas in LoD_3, leakage is assumed to occur at the midpoint of the merged zones, significantly changing the buoyancy-driven airflow.

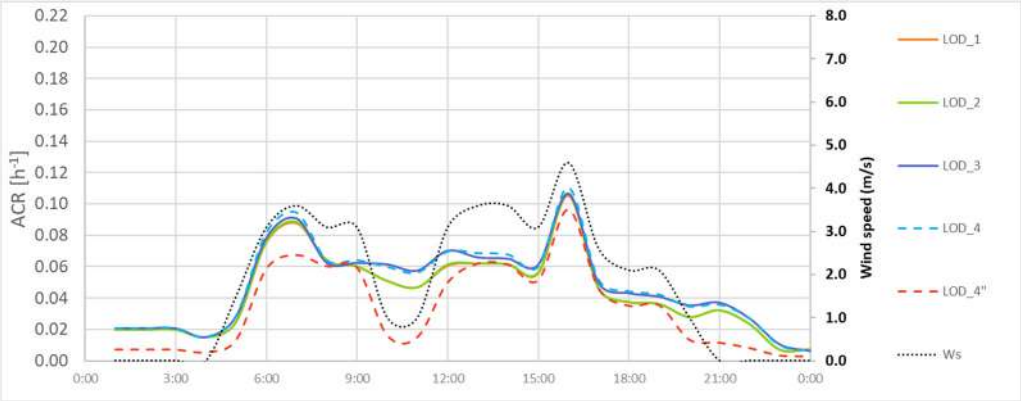

Figure 10. Hourly LoD effect on ACR (winter) for the midrise prototype building.

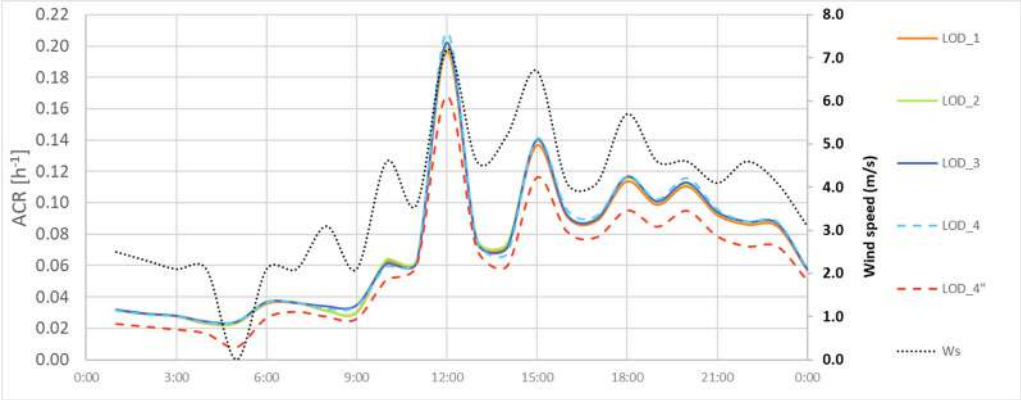

Figure 11. Hourly LoD effect on ACR (summer) for the midrise prototype building.

In LoD_4, where the corridor is removed and the shafts are merged into a single shaft, the ACR values became slightly higher compared to LoD_3. However, the results of LoD_4″, a variation of LoD_4 where leakages from internal floors and roofs are excluded as it is assumed in the three-zone lumped-parameter model, are generally lower than all LoD steps. The average daily building ACR with floor and roof leakage (LoD_4) is 1.5 times higher in winter and 1.2 in summer compared to LoD_4″.

The hourly absolute difference is provided in Figure 12 by directly comparing LoD_1 with LoD_4, and LoD_1 with LoD_4″ (which excludes the roof leakage). The hourly trend reveals that in winter, the error increases as wind speed decreases, while in summer, the error mostly followed the hourly wind speed trend. Moreover, the results demonstrate that excluding floor and roof leakage significantly impacts the ACR values by underestimating the ACR of a detailed model (LoD1).

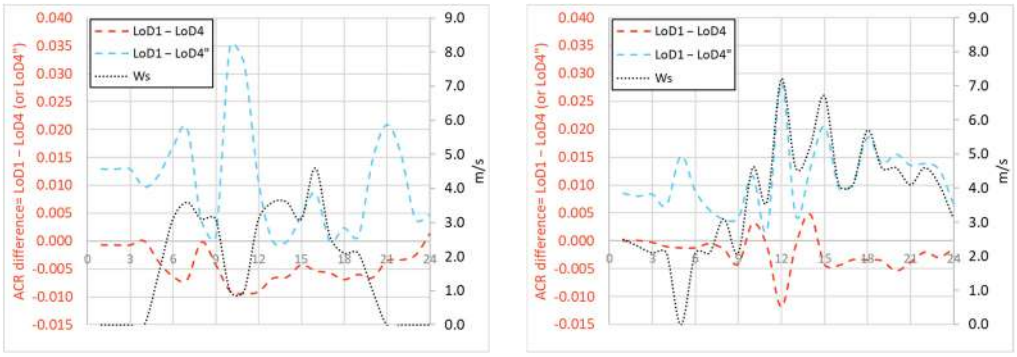

Figure 12. Hourly ACR difference comparing LoD_1 with LoD_4 (in red) and LoD_1 with LoD_4″ (in blue) for the midrise prototype building.

For LoD_4, the average daily MAE is 0.005 h^{-1} and 0.003 h^{-1} for winter and summer respectively, while for LoD_4″, the MAE" increases to 0.01 h^{-1} in both seasons. Using MAPE, the average daily error with floor and roof infiltrations included is 12% and 4% for winter and summer respectively, while excluding the infiltrations from the floor and roof resulted in 35% and 18% MAPE. Given that ACR measurements are low in magnitude, the MAE provides the error values in the actual units and avoids errors' overestimation that occur with MAPE when small differences are compared. Thus, the comparison of ACR values in the following sections is made using the MAE.

4.1.2. Turin Building Results

The LoD results for the building in Turin closely resemble those for the prototype building, with the most significant difference occurring in LoD_3 and LoD_4 as represented in Figures 13 and 14 for winter and summer, using Turin weather data. Like the prototype building, merging the floors into two levels, from LoD_2 to LoD_3, alters the buoyancy effect, resulting in higher ACR values. Moreover, the building in Turin showed low ACR results when the partition between the two apartments is removed: from LoD_3 to LoD_4.

Excluding the leakage from floors and roof (LoD_4″) results in considerable decrease in ACR values in this building; the average daily ACR with roof leakage (LoD_4) is 1.8 higher in winter and 1.6 in summer compared to the LoD_4″.

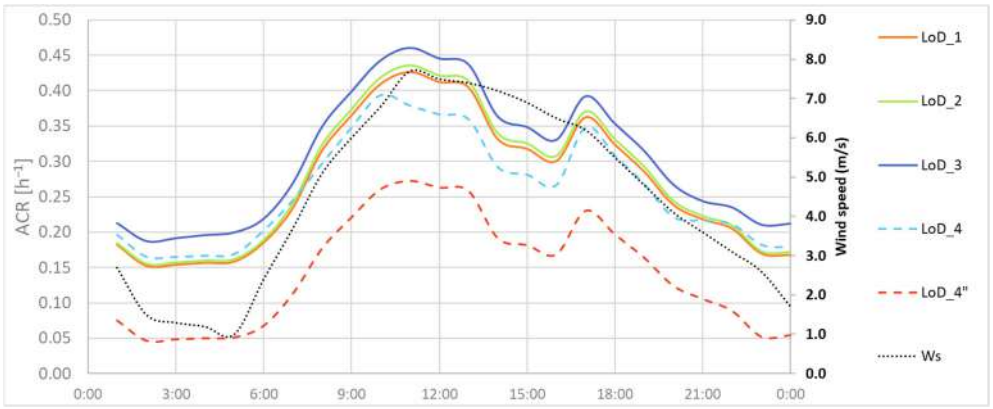

Figure 13. Hourly LoD effect on ACR (winter) for the building in Turin.

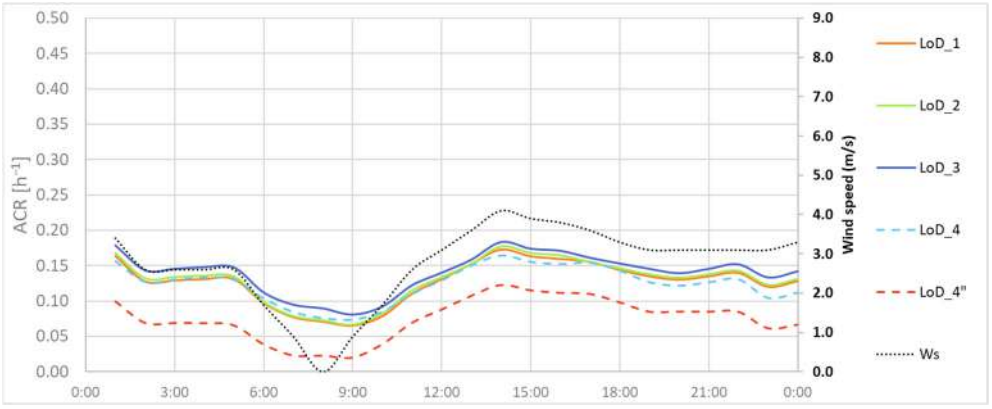

Figure 14. Hourly LoD effect on ACR (summer) for the building in Turin.

Figure 15 presents the hourly ACR difference between the detailed model LoD1 and the three-zone model (LoD_4 and LoD_4″)

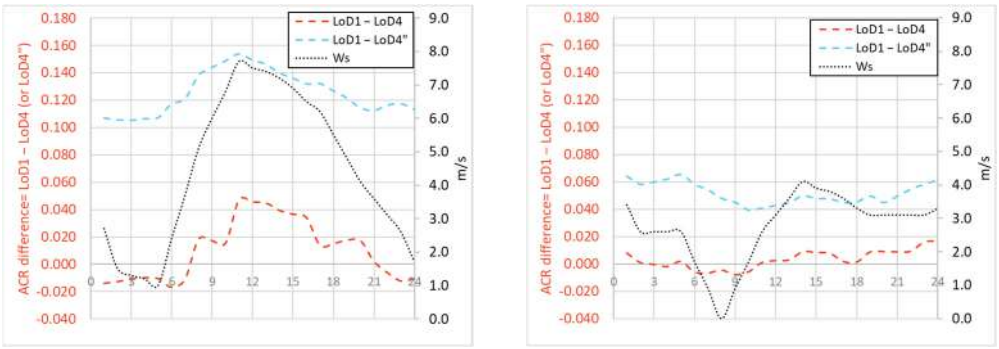

MAE (winter) MAE (summer)

Figure 15. Hourly ACR difference comparing LoD_1 with LoD_4 (in red) and LoD1 with LoD_4″ (in blue) for the building in Turin.

Excluding floor and roof leakage (LoD_4″) significantly reduces the ACR values resulting in underestimation for the building in Turin. Comparing LoD_1 with LoD_4, the MAE for average daily building ACR is 0.02 h^{-1} and 0.006 h^{-1} for winter and summer respectively, while for LoD_4″, the MAE increases to 0.1 h^{-1} and 0.05 h^{-1}. Accounting for roof infiltration, by adding airflow links for the roof in zone b and c, would increase the ACR, improving the simplified model's alignment with the detailed one. This can be done by introducing two flow elements in Equation (3), i.e., $\dot{m}_{br}$ and $\dot{m}_{cr}$ with the correct flow coefficients (C).

4.1.3. Summary

When each building was tested under different climate conditions, the overall trend in results remained unchanged, indicating that building zoning primarily determined the accuracy of the simplified model (LoD_4) compared to the detailed model (LoD_1). The mid-rise building, which included a corridor and two shafts in the detailed model, had different results compared to Turin building, which had no corridor and only a single shaft. While the mid-rise building overestimated the ACR in the three-zone model in both climates, the Turin building underestimated it, considering the average daily ACR.

Overall, the LoD analysis results for both buildings indicate a good balance between the ACR differences observed between LoD_1 and LoD_4, despite the simplification of a detailed building into only three representative zones. These findings suggest that this simplified approach is effective for representing building volumes across a city, provided

that all leakage elements are accurately calculated (as in LoD_4). This finding offers a practical and efficient for urban-scale simulations.

4.2. Three-Zone Lumped-Parameter Model Validation with CONTAM

For the validation, the building in Turin was used to test 10 various indoor/outdoor air temperature scenarios under 12 wind speed conditions. Table 4 presents the MAE values comparing the three-zone lumped-parameter model with the three-zone CONTAM model.

Table 4. The absolute difference in ACR [h^{-1}] between three-zone CONTAM and lumped-parameter model for the tested weather conditions.

[°C]	T_{out}	−10	−5	0	3	7	12	24	28	30	34
	T_{in}	20							26		
	T_{shaft}	2	5	8	9.8	12.2	15.2	24.8	27.2	28.4	30.8
	ΔT $\lvert T_{out} - T_{in} \rvert$	30	25	20	17	13	8	2	2	4	8
Wind speed [m/s]	0.1	0.0005	0.0004	0.0016	0.0026	0.0044	0.0071	0.0128	0.0159	0.0154	0.0151
	0.5	0.0005	0.0004	0.0016	0.0017	0.0005	0.0007	0.0063	0.0095	0.0106	0.0132
	1	0.0036	0.0023	0.0008	0.0002	0.0019	0.0023	0.0053	0.0066	0.0103	0.0067
	2	0.0132	0.0108	0.0049	0.0066	0.0047	0.0030	0.0036	0.0042	0.0049	0.0066
	3	0.0309	0.0107	0.0056	0.0092	0.0081	0.0075	0.0006	0.0013	0.0021	0.0037
	4	0.0099	0.0156	0.0120	0.0128	0.0120	0.0111	0.0053	0.0027	0.0016	0.0004
	5	0.0408	0.0168	0.0179	0.0171	0.0160	0.0149	0.0081	0.0079	0.0066	0.0039
	6	0.0457	0.0243	0.0225	0.0216	0.0203	0.0189	0.0101	0.0093	0.0090	0.0085
	7	0.0448	0.0294	0.0274	0.0263	0.0248	0.0231	0.0122	0.0112	0.0107	0.0098
	8	0.0373	0.0349	0.0326	0.0313	0.0296	0.0275	0.0145	0.0132	0.0126	0.0114
	9	0.0434	0.0406	0.0379	0.0364	0.0344	0.0321	0.0168	0.0153	0.0146	0.0132
	10	0.0496	0.0465	0.0435	0.0417	0.0395	0.0368	0.0193	0.0176	0.0167	0.0151

The results indicate that at lower wind speeds, the absolute differences of ACR are generally low, particularly when the temperature difference is high (e.g., in winter). As wind speed increases, the error rises across all temperature scenarios, with a more obvious effect in winter. For instance, at ΔT = 30 °C, the error is significantly higher at a wind speed of 2 m/s compared to 0.1 m/s. Beyond 5 m/s, the error stabilizes across different temperatures, ranging from 0.014 h^{-1} to 0.05 h^{-1}, suggesting a low influence of temperature differences on ACR estimation. Wind speeds higher than 5 m/s are generally extreme cases in high-density urban environments. Considering the average wind speed for winter and summer in Turin were 1.26 m/s and 1.58 m/s, respectively, for the period 2015–2023, our analysis shows that the lumped-parameter model could be applied with relatively low errors in Turin.

Overall, the absolute differences remain low, with a maximum of 0.05 h^{-1} across all tested weather conditions. These findings demonstrate that the implemented model performs effectively with optimized *fsolve* settings for reduced simulation costs. The model reliably estimates ACR under varying weather conditions, making it a suitable and practical tool for large-scale infiltration analysis in urban environments.

4.3. Field of Application Analysis

The three-zone model presented in this work is applicable to certain building configurations, based on the assumptions of the lumped-parameter model. It is particularly

suitable for buildings located in continuous urban canyons with homogeneous building height, as commonly found in Turin and in city centers generally. This approach, detailed in Section 3.3.2, involves categorizing urban canyons into specific H/W classes to facilitate CFD simulations of airflows in the urban canyon. As a result, the model is not suitable for detached buildings. In such configurations, the lack of neighboring structures on all sides complicates the application of CFD simulations. This is because, in detached buildings, boundary conditions for the simulations become more challenging to define. Consequently, CFD simulations in these scenarios would be less efficient and less representative of urban-scale dynamics, making this model unsuitable for detached buildings.

Moreover, the results of the LoD analysis indicate that the most significant changes occur when the building is simplified into two representative zones for the apartments, which substantially alter the buoyancy effect. This finding makes the model more suitable for low-rise buildings, as applying such simplifications to high-rise buildings can modify the buoyancy effect significantly, potentially leading to inaccuracies in ACR calculations.

Figure 16 illustrates the airflow connection heights for LoD_1 and LoD_4, emphasizing the impact of building height in the simplified model. The variations in airflow opening heights representing the upper and lower zones highlight how simplifying a high-rise building into just three zones can intensify discrepancies in the buoyancy effect.

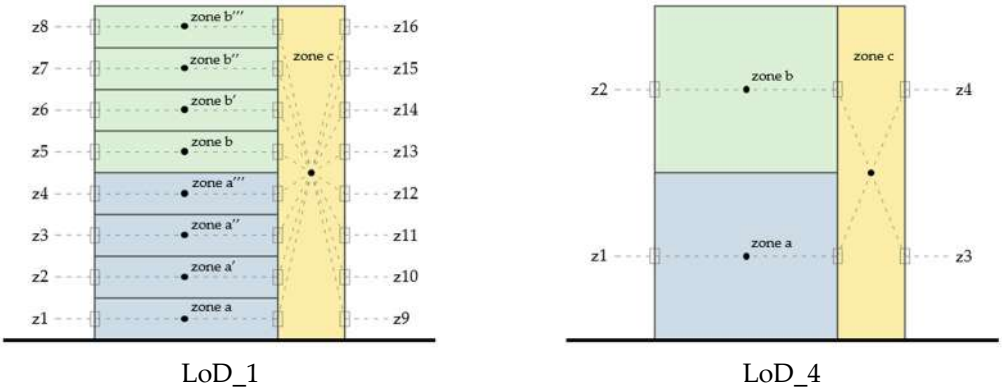

Figure 16. Airflow element heights in the detailed and schematized building models.

Figures 17 and 18 presents the hourly ACR for LoD_1 and LoD_4 for a typical winter and summer day considering different building heights. The results demonstrate that as building height increases, the ACR value decreases. This trend aligns with findings in the literature [35,36] and can be also attributed to the reduced surface-to-volume (S/V) ratio in taller buildings, which lowers the heat loss surface area.

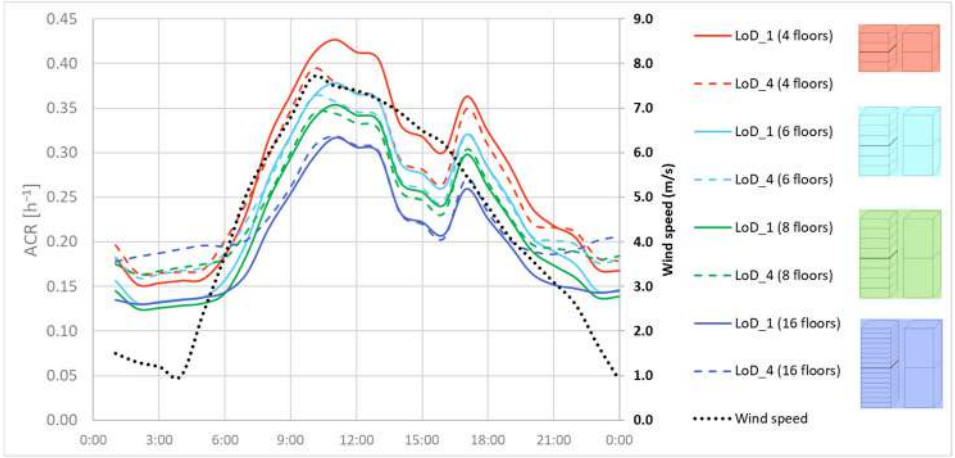

Figure 17. Hourly LoD effect on ACR (winter) considering different building heights.

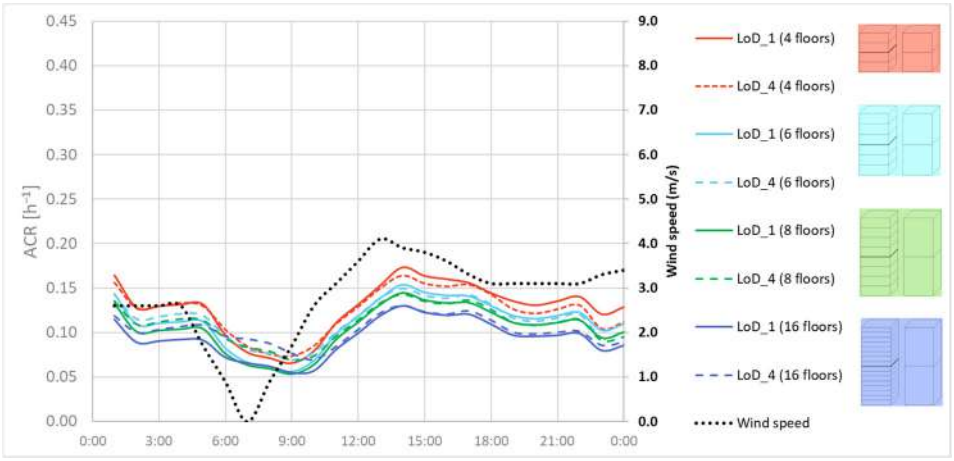

Figure 18. Hourly LoD effect on ACR (summer) considering different building heights.

For the detailed building model, LoD_1, the average daily ACR decreased by 26% in winter and 27% in summer when comparing a 16-story building with a 4-story building. While considering the three-zone model, LoD_4, this decrease is 13% in winter and 18% in summer when comparing a 16-story building with a 4-story one.

Figure 19 provides the absolute difference between LoD_1 and LoD_4 for each analyzed building height. The data clearly shows that shorter buildings generally yield lower differences, which becomes higher under low wind speed conditions. The average daily MAE increases significantly with taller buildings; 1.4 times higher MAE for both winter and summer when comparing a 16-story building with a 4-story one.

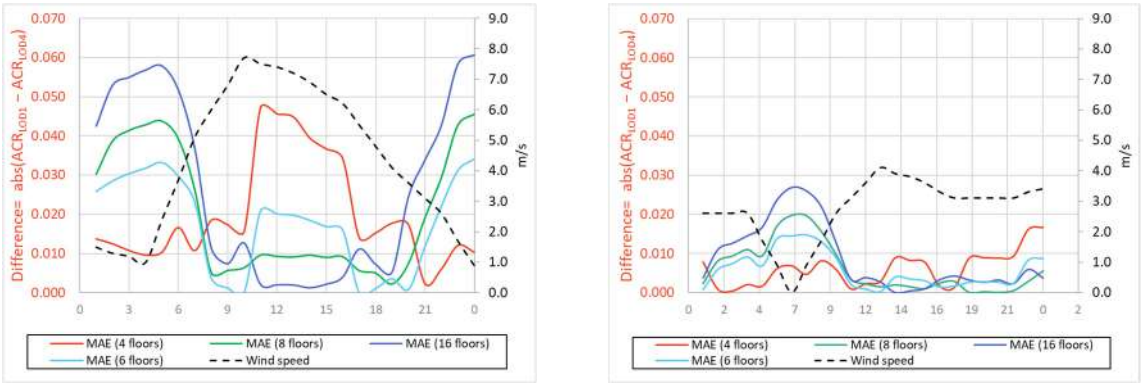

(winter) (summer)

Figure 19. Absolute ACR difference comparing LoD_1 and LoD_4 for different building heights.

The three-zone model was initially designed for residential buildings, which are generally not high-rise structures. Improving the three-zone model for high rise buildings would primarily require detailing the airflow elements for zone c (shaft), which would complicate the system of nonlinear equations (Equations (3) and (4)). A comprehensive analysis on the effect on building internal zones on the ACR results, has shown that the contribution of the number of internal zones on ACRs is higher than detailing of the airflow elements across the façade [37].

Overall, the results showed higher errors for the 16-story building compared to the 4-story building, however the average daily MAE between the LoD_1 and LoD_4 of a 16-story building is 0.03 h^{-1} in winter and 0.01 h^{-1} in summer. This MAE would still be accepted for urban scale applications if needed.

4.4. Example Application: Energy Consumption for Space Heating

4.4.1. Selected Building

In this section, the methodology of the three-zone lumped-parameter model, previously presented, is applied to an hourly GIS-based engineering model for calculating the energy consumption for space heating in residential buildings [6]. Among the buildings examined, a case study building with available hourly consumption data has been selected.

The objective of this application is to evaluate the contribution of the hourly ACR as input data for the energy model, compared to using a constant ACR value, in estimating hourly energy consumption. Both will be compared to the real heating season consumption data during the examined period.

First, the case study building was selected from the zones in the city of Turin that correspond to the application field of the presented methodology. The chosen building is located close to the city center of Turin, built between 1919 and 1945, and has available real hourly energy consumption data. As shown in Figure 20, the examined building is in a narrow canyon, oriented NE-SW (30°N), and positioned on the left side of the canyon. The hourly energy consumption data were collected from the local district heating company and correspond to the heating season of 2022–2023 (15 October 2022–15 April 2023).

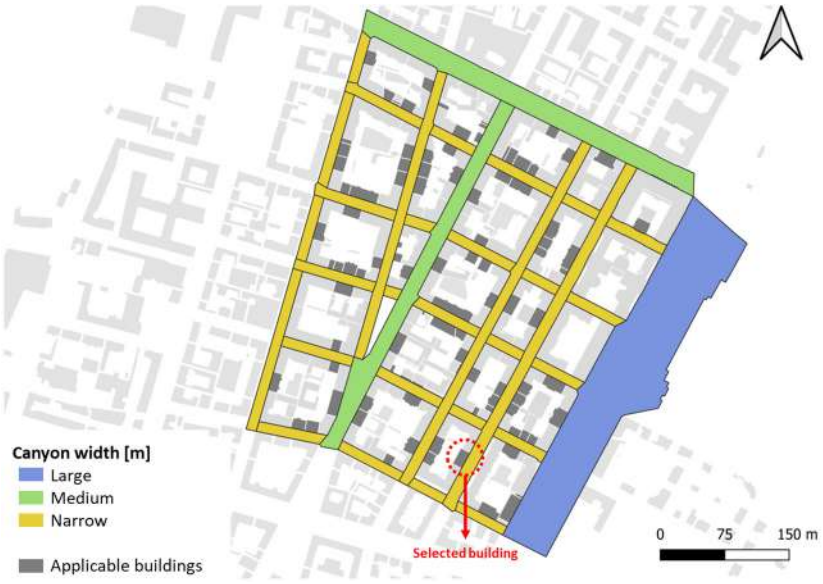

Figure 20. The examined building located in a narrow canyon, NE-SW (30°N) oriented, and left positioned.

Mutani et al. (2020) provided a detailed description of a dynamic engineering model with three thermodynamic systems (TSs), which form the foundation of the GIS-based UBEM [6]. In line with this work, the main input data for the hourly energy consumption model can be summarized into three key categories: building characteristics, local weather data, and heating schedule.

- Building characteristics including the construction period (i.e., 1919–1945), the associated ACR value, and thermal properties, such as thermal capacity (C_t) and thermal transmittance (U) for both opaque (walls, roof, ground) and transparent (glazing) building envelopes, the window-to-wall ratio (WWR), heating system efficiency (η). Reference data are provided in Table 5, with the selected building's construction period highlighted.
- Local weather data includes hourly outdoor air temperature, humidity, pressure, solar radiation, and sun altitude, recorded by the weather station of Politecnico di Torino [38]

for the period from May 2022 to April 2023, in which the hourly consumption data are available.

- Heating schedule, which details the building's occupancy patterns and the operation of the centralized heating system. In the analyzed scenarios, the system operates according to national and local regulations, with the internal air temperature of 19 °C during the day from 6 am to 9 pm with two interruptions at 9 am and 2 pm.

Table 5. Thermo-physical characteristics and ACR values according to construction period.

Period	WALL		ROOF	GROUND	GLAZING			ACR	η
	$C_{envelope}$	U_{wall}	U_{roof}	U_{floor}	U_g	WWR	g-Value	h^{-1}	
	$kJ \cdot m^{-2} \cdot K^{-1}$	$W \cdot m^{-2} \cdot K^{-1}$	$W \cdot m^{-2} \cdot K^{-1}$	$W \cdot m^{-2} \cdot K^{-1}$	$W \cdot m^{-2} \cdot K^{-1}$	-	-	-	-
<1918	504	1.45	1.80	1.75	4.85	0.13	0.85	0.5	0.78
1919–45	**504**	**1.35**	**1.80**	**1.58**	**4.75**	**0.13**	**0.85**	**0.5**	**0.78**
1946–60	283	1.18	1.80	1.23	4.40	0.20	0.85	0.5	0.78
1961–70	283	1.13	2.20	1.30	4.90	0.20	0.85	0.5	0.79
1971–80	257	1.04	2.20	1.00	3.80	0.25	0.75	0.5	0.80
1981–90	264	0.78	1.18	0.95	3.80	0.20	0.75	0.5	0.82
1991–00	274	0.7	0.68	0.80	2.15	0.20	0.67	0.5	0.84
2001–05	274	0.7	0.68	0.80	2.15	0.20	0.67	0.3	0.84
2006–12	267	0.42	0.38	0.41	2.60	0.20	0.50	0.3	0.92
2013–15	267	0.34	0.30	0.33	2.20	0.20	0.50	0.3	0.92
2016–19	267	0.30	0.25	0.30	1.80	0.20	0.35	0.3	0.92

4.4.2. Application Results

This section provides the results of the hourly energy consumption model, considering the scenarios presented in Table 6. All scenarios are then compared to the real consumption data of the case study building.

Table 6. Infiltration scenarios and ACR.

	Scenario	Building Permeability	ACR
1	*cons*	Based on construction period	0.5 constant during the day
2	*cons+(d&n)*	Same as 1, with less permeability during the night for window shutters	0.5 during the day and 0.3 during the nigh
3	*cons+(d&n)+W*	Same as 2, with additional window opening for three times of the day	For 3 h, with windows opening, ACR was calculated by a correlation [6] considering 15 min of windows opening
4	*hourly*	Air infiltration depends on the weather conditions. It was considered an average airtightness of masonry buildings, i.e., 4.58 $L/s/m^2$ @75	ACR was calculated from the three-zone lumped-parameter model in each hour of the year

In the constant scenario "*cons*", the ACR for the analyzed building is set at 0.5 h^{-1}, based on its construction period (see Table 5). In the second scenario "*cons+(d&n)*" a day-night variation is introduced to account for closed window shutters at night by reducing the ACR to 0.3 h^{-1} from 9 p.m. to 8 a.m. In the third scenario "*cons+(d&n)+W*", window shutters are closed at night and windows are opened for 15 min three times per day [6].

The final scenario uses the hourly ACR (named "*hourly*") as a result of the three-zone lumped-parameter model presented previously, with an airtightness value of 4.58 $L/s/m^2$

@75 Pa, representing the average airtightness for masonry buildings based on a sample of 152 buildings [22].

The main output of the energy model is the heat loss through ventilation (Q_v) [kWh], which directly depends on the ACR values. Figure 21a,b provide Q_v for selected days during the heating season, comparing the different analyzed ACR scenarios for two representative days. Figure 21c,d present the hourly energy consumption for space heating for the same days.

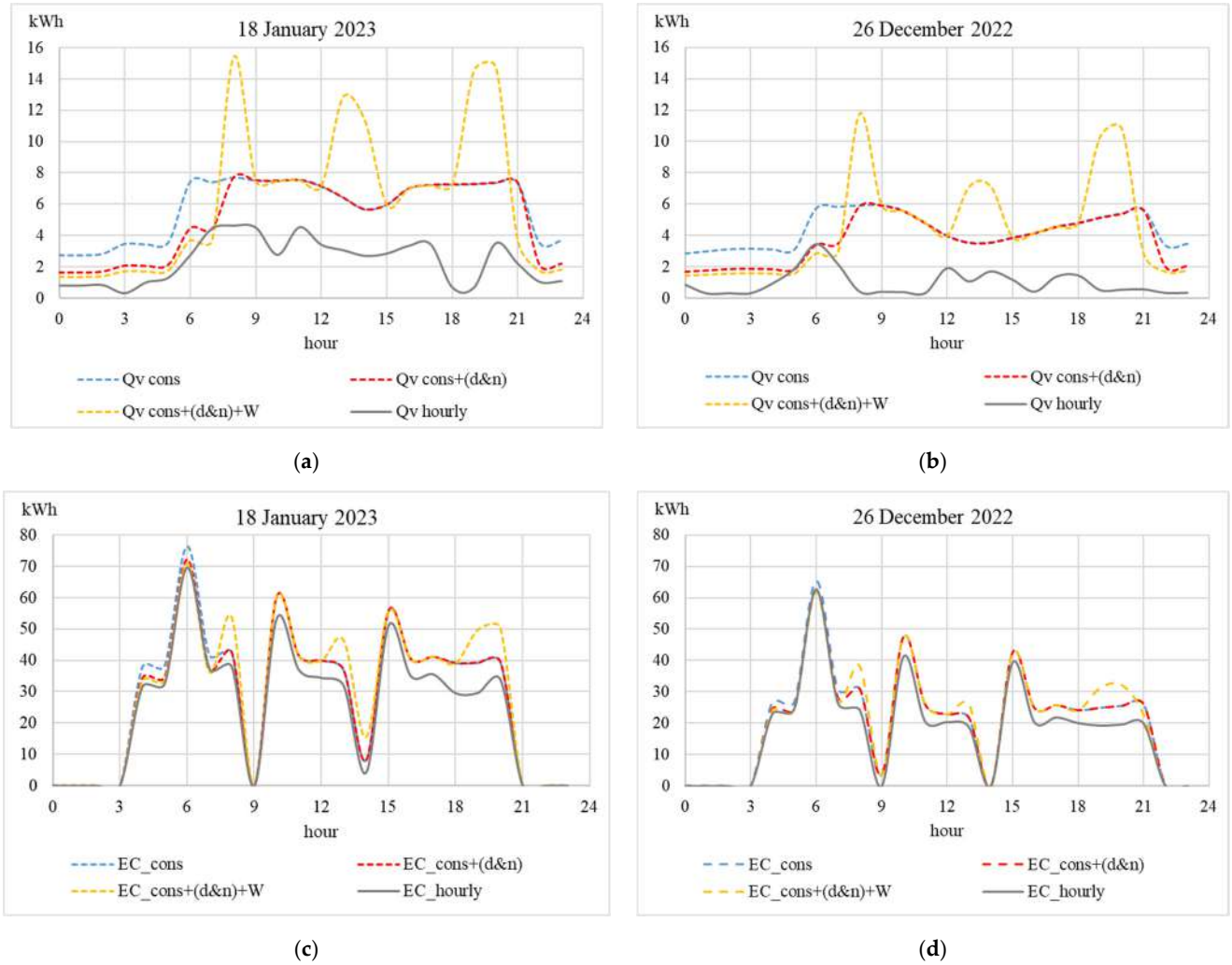

Figure 21. Hourly heat loss by ventilation Q_V [kWh] (**a**,**b**) and hourly energy consumption (EC) for space heating (**c**,**d**) for selected days in the heating season for the analyzed scenarios.

By examining the hourly profiles of the ventilation load in Figure 21a,b, it is evident that all constant ACR scenarios, particularly *cons+(d&n)+W*, show higher values compared to the *hourly* ACR scenario. This suggests that the *hourly* ACR scenario may be influenced by: the wind speed adjustment within the urban canyon (which is low), the low infiltration value used in the three-zone lumped-parameter model (which could not reflect the real situation), and finally the lack of roof infiltration considered in the three-zone lumped-parameter model.

As seen in Figure 21c,d, the energy consumption using the *hourly* ACR scenario shows, overall, lower values compared to the other three scenarios that use constant ACR. This demonstrates the direct impact of building ACR on space heating energy consumption.

Figure 22 shows the calculated and measured energy consumption for selected days in each month of the heating season. As this engineering model is directly influenced by

the building physical characteristics and weather data, the use of hourly ACR presents a more accurate approach compared to fixed values, especially with natural ventilation.

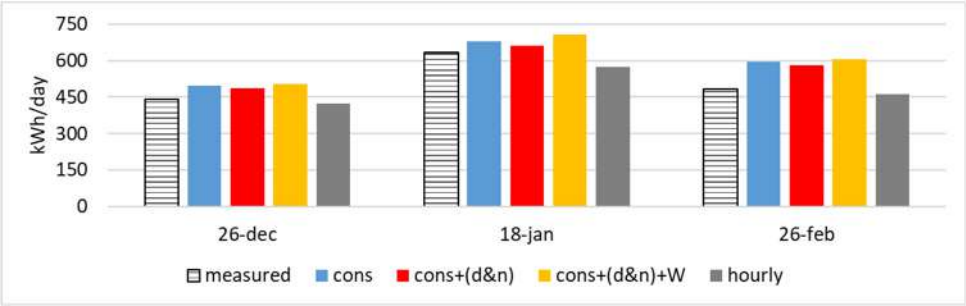

Figure 22. Daily energy consumption for space heating representative days during the heating season comparing the ACR scenarios and the measured consumption data.

For each scenario and day examined in Figure 22, Table 7 provides the MAPE. Among the analyzed scenarios, the *hourly* MAPE was lower, indicating that the three-zone lumped-parameter model provided better estimates of the ACR values. However, the *cons+(d&n)* scenario showed the lowest MAPE for 18 January, highlighting the role of unpredictable user behavior or system performance. Generally, on the analyzed days, MAPE results were low under conditions of low wind speed, aligning with the findings previously presented in Table 4.

Table 7. MAPE of the different ACR scenarios in predicting the daily energy consumption for space heating in representative days of the heating season.

Scenario	26-Dec	18-Jan	26-Feb
cons	12.6%	7.2%	22.9%
cons+(d&n)	10.3%	4.7%	19.6%
cons+(d&n)+W	14.5%	11.9%	25.4%
hourly	4.3%	7.6%	4.7%
Tout [°C]	6.83	5.44	5.96
Ws [m/s]	1.88	0.97	1.93

Figure 23 compares the hourly energy consumption for space heating [kWh] using both the *cons* ACR (solid red line) and *hourly* ACR (dotted red line), against the measured hourly consumption (dashed red line) for two selected days during the heating season. The figures also provide other relevant heat losses and gains [kWh] in the energy consumption model, which are: the heat loss by ventilation Q_v (blue line), the heat gain by internal gains Q_I (violet line), the heat loss by transmission from opaque envelope $Q_{t,e}$ (light green line), the heat loss by transmission from transparent envelope $Q_{t,g}$ (dark green line), the heat gain by solar irradiation Q_{sol} (yellow line). In addition, the solar irradiance $I_{sol,h}$ [$W \cdot m^{-2}$] is also shown (dotted orange line).

Analyzing the two graphs, both the *cons* and *hourly* ACR scenarios align closely with the real measured data (dashed red line), but generally the *cons* scenario overestimates the consumption compared to the *hourly* scenario. However, as provided previously in Table 7, the average daily MAPE for the presented two days in Figure 23 was lower for the *hourly* scenario in December and slightly lower for *cons* scenario in January.

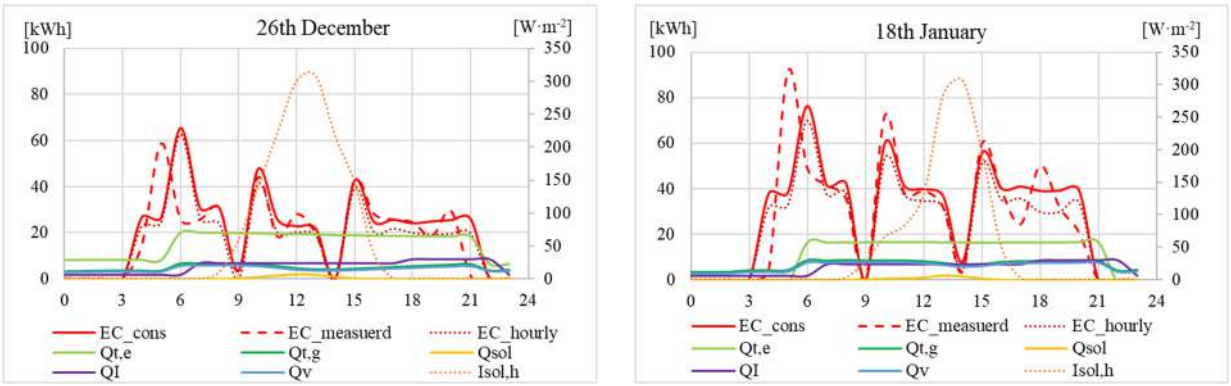

Figure 23. Hourly profiles of the energy consumption for space heating for selected two days comparing the measured data (dashed red line) with the ACR constant (solid red line) and the ACR hourly (dotted red line) scenarios.

Generally, the *hourly* scenario is underestimating energy consumption compared to the real measured data, which could be highly associated with the lack of roof infiltration in the current three-zone lumped parameter model. As mentioned earlier, the three-zone lumped-parameter model used in this study simplifies the building geometry by excluding infiltration from the roof and internal floors. This simplification was done to reduce simulation costs when solving the system of nonlinear equations. However, the model can be improved to include two extra links to the current system of nonlinear equations (Equation (3)) to account for roof infiltration from zones b and c. Nevertheless, the relatively small difference between the measured energy consumption and the consumption based on the *hourly* ACR, as presented in Figure 23, suggests that this methodology is promising. It effectively accounts for the influence of the built environment and corrected wind speed, which are critical for analyzing building airflow from natural ventilation and estimating energy consumption at urban scale.

5. Conclusions

This study assesses the accuracy of a steady-state three-zone lumped-parameter model by analyzing first the effect of simplifying a building into three-zones and then by validating the implemented three-zone lumped-parameter model with a three-zone CONTAM model. The lumped-parameter model accounts for natural infiltration in buildings and incorporates the effects of the surrounding environment by adjusting outside wind speed within urban canyons using CFD simulations for defined urban canyon and weather scenarios.

The comparison across different LoDs revealed that while internal partitions had a minor impact, simplifications—such as merging floors into representative zones—had a greater influence on ACR values, particularly by altering the buoyancy effect. Additionally, the exclusion of infiltration through floors and roofs led to a notable reduction in ACR, emphasizing the significance of including these elements in building infiltration modeling. The effect of including leakages from the floor and roof on the average daily building ACR was found to be 1.5 times higher in winter and 1.2 in summer for the prototype building, while for the building in Turin it was 1.8 times higher in winter and 1.6 in summer.

The results of comparing the three-zone lumped-parameter model with CONTAM using the building in Turin showed higher MAE in winter, with higher wind speed and higher ΔT.

Applying this model to a real case study and comparing its results with measured data confirmed that ACR values derived from the three-zone lumped-parameter model were lower compared to the constant ACR value. This finding underscores the necessity of accounting for all infiltration elements in buildings to improve model accuracy.

Despite these limitations, the proposed three-zone lumped-parameter model remains a computationally efficient tool for estimating ACR in urban-scale energy modeling. Future enhancements—such as refining the representation of infiltration pathways—could further improve its accuracy. These refinements hold significant potential in enabling more accurate assessments of ACR from natural ventilation at urban scale, which plays a crucial role in building energy loads. The ultimate goal in enhancing energy consumption modeling is to develop effective strategies for utilizing energy tailored to dense urban environments.

Author Contributions: Conceptualization, G.M. and S.S.; methodology, G.M. and S.S.; software, Y.U.; validation, Y.U.; formal analysis, Y.U.; investigation, L.N. and G.M.; resources, G.M.; data curation, S.S.; writing—original draft preparation, Y.U. and S.S.; writing—review and editing, G.M. and L.N.; visualization, Y.U.; supervision, G.M. All authors have read and agreed to the published version of the manuscript.

Funding: This research received no external funding.

Data Availability Statement: The raw data supporting the conclusions of this article will be made available by the authors on request.

Conflicts of Interest: The authors declare no conflict of interest.

References

1. IEA. Buildings—Energy System. Available online: https://www.iea.org/energy-system/buildings (accessed on 28 January 2025).
2. NREL Researchers Reveal How Buildings Across United States Do—and Could—Use Energy. Available online: https://www.nrel.gov/news/features/2023/nrel-researchers-reveal-how-buildings-across-the-united-states-do-and-could-use-energy.html (accessed on 28 January 2025).
3. U.S Department of Energy. Building Energy Modeling. Available online: https://www.energy.gov/eere/buildings/building-energy-modeling (accessed on 28 January 2025).
4. Ali, U.; Shamsi, M.H.; Hoare, C.; Mangina, E.; O'Donnell, J. Review of urban building energy modeling (UBEM) approaches, methods and tools using qualitative and quantitative analysis. *Energy Build.* **2021**, *246*, 111073. [CrossRef]
5. Kamel, E. A Systematic Literature Review of Physics-Based Urban Building Energy Modeling (UBEM) Tools, Data Sources, and Challenges for Energy Conservation. *Energies* **2022**, *15*, 8649. [CrossRef]
6. Mutani, G.; Todeschi, V.; Beltramino, S. Energy Consumption Models at Urban Scale to Measure Energy Resilience. *Sustainability* **2020**, *12*, 5678. [CrossRef]
7. Javanroodi, K.; Mahdavinejad, M.; Nik, V.M. Impacts of urban morphology on reducing cooling load and increasing ventilation potential in hot-arid climate. *Appl. Energy* **2018**, *231*, 714–746. [CrossRef]
8. Santantonio, S.; Mutani, G. QGIS-Based Tools to Evaluate Air Flow Rate by Natural Ventilation in Buildings at Urban Scale. In Proceedings of the BSA Conference 2022 IBPSA-Italy, Bozen-Bolzano, Italy, 29 June–1 July 2022; Volume 5, pp. 331–339. Available online: https://publications.ibpsa.org/conference/paper/?id=bsa2022_9788860461919_42 (accessed on 6 January 2025).
9. Todeschi, V.; Boghetti, R.; Kämpf, J.H.; Mutani, G. Evaluation of Urban-Scale Building Energy-Use Models and Tools—Application for the City of Fribourg, Switzerland. *Sustainability* **2021**, *13*, 1595. [CrossRef]
10. Dabirian, S.; Panchabikesan, K.; Eicker, U. Occupant-centric urban building energy modeling: Approaches, inputs, and data sources—A review. *Energy Build.* **2022**, *257*, 111809. [CrossRef]
11. Taddeo, P.; Ortiz, J.; Salom, J.; Segarra, E.L.; González, G.V.; Ruiz, G.R.; Bandera, C.F. Comparison of Experimental Methodologies to Estimate the Air Infiltration Rate in a Residential Case Study for Calibration Purposes, 2018. Available online: https://www.semanticscholar.org/paper/Comparison-of-experimental-methodologies-to-the-air-Taddeo-Ortiz/437eab49b3304179d102167876f74733caff6be4 (accessed on 28 January 2025).
12. Santantonio, S.; Dell'Edera, O.; Moscoloni, C.; Bertani, C.; Bracco, G.; Mutani, G. Wind-driven and buoyancy effects for modeling natural ventilation in buildings at urban scale. *Energy Effic.* **2024**, *17*, 95. [CrossRef]
13. National Institute of Standards and Technology. CONTAM Introduction. Available online: https://www.nist.gov/el/energy-and-environment-division-73200/nist-multizone-modeling/software/contam (accessed on 15 December 2024).
14. Ng, L.C.; Musser, A.; Persily, A.K.; Emmerich, S.J. *Airflow and Indoor Air Quality Models of DOE Prototype Commercial Buildings*; National Institute of Standards and Technology: Gaithersburg, MD, USA, 2019. [CrossRef]

15. Dols, W.S.; Polidoro, B. *CONTAM User Guide and Program Documentation Version 3.4*; National Institute of Standards and Technology: Gaithersburg, MD, USA. Available online: https://www.nist.gov/publications/contam-user-guide-and-program-documentation-version-34 (accessed on 18 December 2024).
16. Haghighat, F.; Megri, A.C. A Comprehensive Validation of Two Airflow Models—COMIS and CONTAM. *Indoor Air* **1996**, *6*, 278–288. [CrossRef]
17. Chung, K.-C. Development and Validation of a Multizone Model for Overall Indoor Air Environment Prediction. *HVAC&R Res.* **1996**, *2*, 376–385. [CrossRef]
18. Emmerich, S.J.; Howard-Reed, C.; Nabinger, S. Validation of multizone IAQ model predictions for tracer gas in a townhouse. *Build. Serv. Eng. Res. Technol.* **2004**, *25*, 305–316. [CrossRef]
19. Emmerich, S.J. *Validation of Multizone IAQ Modeling of Residential-Scale Buildings: A Review*; No. Pt.2; National Institute of Standards and Technology: Gaithersburg, MD, USA, 2001; Volume 107. Available online: https://www.nist.gov/publications/validation-multizone-iaq-modeling-residential-scale-buildings-review (accessed on 18 December 2024).
20. Ng, L.C.; Zimmerman, S.M.; Good, J.; Tool, B.; Emmerich, S.; Persily, A. *Estimating Real-Time Infiltration for Use in Residential Ventilation Control*; National Institute of Standards and Technology: Gaithersburg, MD, USA, 2019. Available online: https://www.nist.gov/publications/estimating-real-time-infiltration-use-residential-ventilation-control (accessed on 18 December 2024).
21. IEA. Annex 23—An International Effort in Multizone Air Flow Modeling | Smarter Small Buildings. Available online: https://smartersmallbuildings.lbl.gov/publications/annex-23-international-effort (accessed on 18 March 2025).
22. RDH Building Science, Study of Part 3 Building Airtightness. Available online: https://www.rdh.com/resource/study-of-part-3-building-airtightness/ (accessed on 9 December 2024).
23. UNI EN 12207:2017—UNI Ente Italiano di Normazione. Available online: https://store.uni.com/uni-en-12207-2017 (accessed on 17 November 2024).
24. Mckeen, P.; Liao, Z. The Influence of Building Airtightness on Airflow in Stairwells. *Buildings* **2019**, *9*, 208. [CrossRef]
25. UNI/TS 11300-1:2014 —Determinazione del Fabbisogno di Energia Termica Dell'edificio per la Climatizzazione Estiva ed Invernale. Available online: https://store.uni.com/uni-ts-11300-1-2014 (accessed on 15 November 2024). (In Italian)
26. EnergyPlus. Available online: https://energyplus.net/weather-location/north_and_central_america_wmo_region_4/USA/FL/USA_FL_Southwest.Florida.Intl.AP.722108_TMY3 (accessed on 16 December 2024).
27. National Institute of Standards and Technology. CONTAM Weather File Creator 2.0. 2018. Available online: https://www.nist.gov/el/energy-and-environment-division-73200/nist-multizone-modeling/software/contam-weather-file (accessed on 24 January 2025).
28. Florida Solar Energy Center; Chandra, S. Procedures for Calculating Natural Ventilation Airflow Rates in Buildings. 03-87. FSEC Energy Research Center®, 1987. Available online: https://stars.library.ucf.edu/fsec/988 (accessed on 16 December 2024).
29. Kent, C.W.; Lindberg, F.; Offerle, B.; Grimmond, S.; Krave, N. Urban Morphology and Morphometric Calculator (Grid), UMEP Documentation, 2023. Available online: https://umep-docs.readthedocs.io/en/latest/pre-processor/Urban%20Morphology%20Morphometric%20Calculator%20(Grid).html (accessed on 17 February 2025).
30. Kent, C.W.; Grimmond, S.; Barlow, J.; Gatey, D.; Kotthaus, S.; Lindberg, F.; Halios, C.H. Evaluation of Urban Local-Scale Aerodynamic Parameters: Implications for the Vertical Profile of Wind Speed and for Source Areas. *Bound.-Layer Meteorol.* **2017**, *164*, 183–213. [CrossRef] [PubMed]
31. Kanda, M.; Inagaki, A.; Miyamoto, T.; Gryschka, M.; Raasch, S. A New Aerodynamic Parametrization for Real Urban Surfaces. *Bound.-Layer Meteorol.* **2013**, *148*, 357–377. [CrossRef]
32. Javanroodi, K.; Nik, V.M. Interactions between extreme climate and urban morphology: Investigating the evolution of extreme wind speeds from mesoscale to microscale. *Urban Clim.* **2020**, *31*, 100544. [CrossRef]
33. Feustel, H.E. COMIS—An international multizone air-flow and contaminant transport model. *Energy Build.* **1999**, *30*, 3–18. [CrossRef]
34. Fsolve. Available online: https://it.mathworks.com/help/optim/ug/fsolve.html (accessed on 10 January 2025).
35. Emmerich, S.J.; Persily, A.; Mcdowell, T. Impact of Infiltration on Heating and Cooling Loads in U.S. Office Buildings, Building and Fire Research Laboratory, National Institute of Standards and Technology. Available online: https://www.researchgate.net/publication/265919110_Impact_of_Infiltration_on_Heating_and_Cooling_Loads_in_US_Office_Buildings (accessed on 10 January 2025).
36. Emmerich, S.J.; Persily, A.K. U.S commercial building airtightness requirements and measurements. In Proceedings of the AIVC Conference 2011, Brussels, Belgium, 12–13 October 2011. Available online: https://www.aivc.org/resource/us-commercial-building-airtightness-requirements-and-measurements (accessed on 30 January 2025).

37. Herring, S.J.; Batchelor, S.; Bieringer, P.E.; Lingard, B.; Lorenzetti, D.M.; Parker, S.T.; Rodriguez, L.; Sohn, M.D.; Steinhoff, D.; Wolski, M. Providing pressure inputs to multizone building models. *Build. Environ.* **2016**, *101*, 32–44. [CrossRef]
38. LivingLAB@polito.it—Ambiente Esterno. Available online: https://smartgreenbuilding.polito.it/monitoraggio/esterno.asp (accessed on 16 December 2024).

Disclaimer/Publisher's Note: The statements, opinions and data contained in all publications are solely those of the individual author(s) and contributor(s) and not of MDPI and/or the editor(s). MDPI and/or the editor(s) disclaim responsibility for any injury to people or property resulting from any ideas, methods, instructions or products referred to in the content.